Interpenetrated Gel Polymer Binder for High-Performance Silicon Anodes in Lithium-ion Batteries

*Jiangxuan Song, Mingjiong Zhou, Ran Yi, Terrence Xu, Mikhail L. Gordin, Duihai Tang, Zhaoxin Yu, Michael Regula, and Donghai Wang**

Silicon has attracted ever-increasing attention as a high-capacity anode material in Li-ion batteries owing to its extremely high theoretical capacity. However, practical application of silicon anodes is seriously hindered by its fast capacity fading as a result of huge volume changes during the charge/discharge process. Here, an interpenetrated gel polymer binder for high-performance silicon anodes is created through in-situ crosslinking of water-soluble poly(acrylic acid) (PAA) and polyvinyl alcohol (PVA) precursors. This gel polymer binder with deformable polymer network and strong adhesion on silicon particles can effectively accommodate the large volume change of silicon anodes upon lithiation/delithiation, leading to an excellent cycling stability and high Coulombic efficiency even at high current densities. Moreover, high areal capacity of ~4.3 mAh/cm^2 is achieved based on the silicon anode using the gel PAA–PVA polymer binder with a high mass loading. In view of simplicity in using the water soluble gel polymer binder, it is believed that this novel binder has a great potential to be used for high capacity silicon anodes in next generation Li-ion batteries, as well as for other electrode materials with large volume change during cycling.

1. Introduction

Lithium-ion batteries (LIBs) have been applied in a variety of portable electronic devices and are being pursued as power sources for hybrid electric vehicles and electric vehicles.[1–13] With respect to the anodes for LIBs, materials that can electrochemically form intermetallic alloys with Li have attracted tremendous attention as anode materials due to their much higher capacities than that of conventional graphite anodes based on intercalation chemistry.[10,14–17] Among these, silicon (Si) is particularly attractive because of its highest known theoretical capacity of ~4200 mAh/g and low charge-discharge potential of ~0.4 V vs Li/Li$^+$.[18–23] In addition, Si is abundant, low-cost, and eco-friendly, which makes it more promising for low-cost, high-energy LIBs. However, the silicon anode materials suffer from substantial volume change (>400%) during lithiation/delithiation. This will cause poor electrical contact of Si particles with the conducting matrix and severe pulverization of the silicon, as well as the excess growth of solid-electrolyte interphase (SEI).[24–31] As a result, the silicon anodes show fast capacity fading, low Coulombic efficiency, and electrode deterioration upon cycling. The situation becomes even worse when fabricating high energy cells where high mass loading of active materials (mg-Si/cm^2) on current collectors is necessary.[32]

Polymer binder, one of the major components in an electrode, is used to bind active materials and conducting particles together onto the current collector. The properties of polymer binders play an important role in the electrochemical performance of the electrodes, especially for the cycle life and irreversible capacity losses.[33–35] Poly(vinylidene fluoride) (PVDF) is a conventional binder and widely used in traditional LIBs because of its acceptable adhesion and wide electrochemical window.[36,37] However, the non-functionalized linear chain structure of the PVDF binder cannot afford sufficient binding to high-capacity anode particles that exhibit huge volume changes.[33,38] This requires improved binding characteristics of binders to enable electrode integrity for long cycling life. Thus, novel polymer binders with the ability to accommodate substantial volume changes during lithiation/delithiation of Si anodes are highly desirable.

Recently, much attention has been devoted to developing functional binders that can improve adhesion on silicon particles. For example, polymer binders that contain carboxyl groups and their derivatives, such as polyacrylic acid (PAA)[39] and carboxymethyl cellulose (CMC) based polymers (e.g., CMC or NaCMC),[38,40] show better electrochemical performance than non-functional polymers such as PVDF and styrene-butadiene rubber (SBR).[39,41] These functional binders show enhanced binding with silicon particles via hydrogen bonding and/or covalent chemical bonds between the polar functional groups of the binder and the partially hydrolyzed surface SiO_2 layer of Si particles. Moreover,

Dr. J. Song, Dr. M. Zhou, R. Yi, Dr. T. Xu, M. L. Gordin, Dr. D. Tang, Z. Yu, M. Regula, Prof. D. Wang
Department of Mechanical and Nuclear Engineering
The Pennsylvania State University, University Park
PA 16802, USA
E-mail: dwang@psu.edu
Dr. M. Zhou
The School of Material Science and Chemical Engineering
Ningbo University
Fenghua Road 818, Jiangbei District, Ningbo 315211, Zhejiang, PR China

DOI: 10.1002/adfm.201401269

multi-functional polymer binders were further developed to enhance the interaction of silicon and binder. For example, high-modulus natural polysaccharidenatural (alginate)[33] containing hydroxyl and carboxyl groups and dopamine-grafted PAA[42] containing catechol and carboxyl groups were developed for high performance silicon anodes. Liu et al.[43] developed a new conductive polymer binder, integrating triethyleneoxide monomethyl ether, methyl benzoate ester, and fluorenone moieties into a single-component n-type conductive polymer for silicon anode materials to improve mechanical adhesion, ductility, and electrolyte-uptake. Indeed, the incorporation of the aforementioned functional groups to the polymer chain presented higher adhesion associated with improved performance of silicon anode. Nonetheless, the linear chain nature of these polymer binders is susceptible to sliding upon the continual volume change of silicon during cycling. As a result, the polymer chain together with the deformed electrode cannot recover to its original state and irreversible change takes place. To combat this, three dimensional polymer networks, including the cross-linked CMC-PAA binder[44] and porous conductive gel polymer[34] were sequentially developed for the silicon anodes, in which the polymer chain was anchored by a cross-linking technique. Another strategy of utilizing self-healing polymer via a hydrogen bonding driving force was also recently adopted for silicon binder.[35] These designs effectively enhanced the electrochemical performance of Si anodes by suppressing the adverse effect from their large volume expansion. Despite promising progress, the current research on polymer binders for silicon is still limited in the following ways. First, most of the literature reported a limited cycling for these binders (≤100 cycles) and a relatively low current density (~400 mA/g), which is far from the practical application that needs at least 300 cycles and fast charge/discharge. Second, low-mass-loading electrodes (<1.0 mg-Si/cm^2) were used for the evaluation of these binders, making these results less attractive for practical application where high mass loading is necessary for the high areal capacity (>4 mAh/cm^2) to advance the energy density of LIBs. Third, less attention has been paid to evaluating the developed binders on silicon-graphite composite anodes that remain a distinct approach for practical application of Si materials in current LIBs.

It is well known that super absorbent resin has an extra-large volume change (up to 500–1000 times) during solvent absorption processes. Most interestingly, it can normally recover to its original state after losing solvent from its three-dimensional flexible network.[45,46] Inspired by this smart flexible polymer gel network, here, we report a novel deformable gel polymer binder for Si anode materials through an in-situ thermal-crosslinking of water soluble poly(acrylic acid) (PAA) and poly(vinyl alcohol) (PVA). This gel polymer binder contains carboxylic and hydroxyl functional groups, and can thus strongly bond with Si particles, exhibiting high mechanical strength of adhesion on Si as well as a particularly recoverable deformation through the reversible morphology change with the silicon particles. This leads to an excellent cycling stability and high Coulombic efficiency even at a high current density (4 A/g) or a high Si mass loading (~2.4 mg-Si/cm^2).

2. Results and Discussion

The silicon electrodes with the interpenetrated gel polymer binder were prepared by an *in-situ* thermo-induced polymerization approach. Commercial silicon nanoparticles in elliptical or spherical shapes with diameters in the range of 30 to 100 nm were used for this study (see Figure S1 in Supporting Information). The silicon nanoparticles were covered with a thin layer of amorphous SiO_2 due to oxidation when exposed to air.[33] This was confirmed by Fourier transform infrared spectroscopy (FTIR) as shown in Figure S2. The spectra show typical vibration bands of silica materials such as the Si–O–Si asymmetric stretching band at 1176 cm^{-1} and Si–O symmetric stretching band at 885 cm^{-1}.[33,44] Moreover, the broad peak located in 3000–3600 cm^{-1} was also clearly observed, which is attributed to the hydrogen bonding of Si-OH groups.[33] All of these characteristic peaks shown in the FTIR spectra support the existence of an SiO_2 layer on the silicon surface, which agrees with previous reports.[33] The aqueous solution of poly(acrylic acid) (PAA) and poly(vinyl alcohol) (PVA) (9:1, weight ratio) was used as polymer precursor for the gel polymer network. The electrodes were fabricated by a coating process of the slurry comprising of 60 wt.% Si nanoparticles and 20 wt.% carbon black, and 20 wt.% gel polymer binder precursor. These electrodes were heated at 100 °C for 5 h and then at 150 °C for another 1 h under vacuum. In this manner, the esterification reaction would take place between the carboxyl functional group of PAA and hydroxyl functional group of PVA. Simultaneously, the carboxylic acid group of PAA would also react with the hydroxyl groups of SiO_2 on the surface of the Si particles to form covalent ester bonds between the Si particles and polymer network.

To verify the chemical structure of the interpenetrated gel polymer binder, FTIR was conducted, as shown in **Figure 1**. After crosslinking PAA with PVA, the stretching vibration peak (~3300 cm^{-1}) of the O–H bond in PVA was decreased and shifted to a lower wavenumber. Moreover, the stretching vibration peaks (1720 cm^{-1}) of C=O band of PAA shifted to a lower wavenumber of 1714 cm^{-1}. These peak changes demonstrated the –COO– formation due to esterification reaction of PAA and PVA, resulting in a cross-linked gel polymer network.[47,48] Furthermore, in the presence of silicon in the interpenetrated gel PAA-PVA binder, the stretching vibration peak of C=O of PAA became broader at a higher wavenumber (1730 cm^{-1}), indicating the occurrence of the condensation reaction between the Si–OH of silicon particles and –COOH of PAA.[16] The strong interactions between the PAA-PVA binder and the Si particles are favorable for improving the electrode integrity and thus mitigating destruction of the electrical network even under a large volume change during cycling, which has been previously identified as one of the most critical factors affecting the stability of Si-based electrodes.[39,43]

The electrochemical properties of the silicon electrodes were evaluated by using CR2016 coin cells with lithium foil as the counter electrode. The charge/discharge processes of the silicon electrodes were performed between 0.01 and 1.5 V by using 1 M $LiPF_6$ in a mixture of ethylene carbonate, diethyl carbonate and dimethyl carbonate (EC: DEC: DMC, 1:1:1 by volume) as electrolyte and fluoroethylene carbonate (FEC, 10 vol.%) as additive. The silicon electrodes containing widely used NaCMC

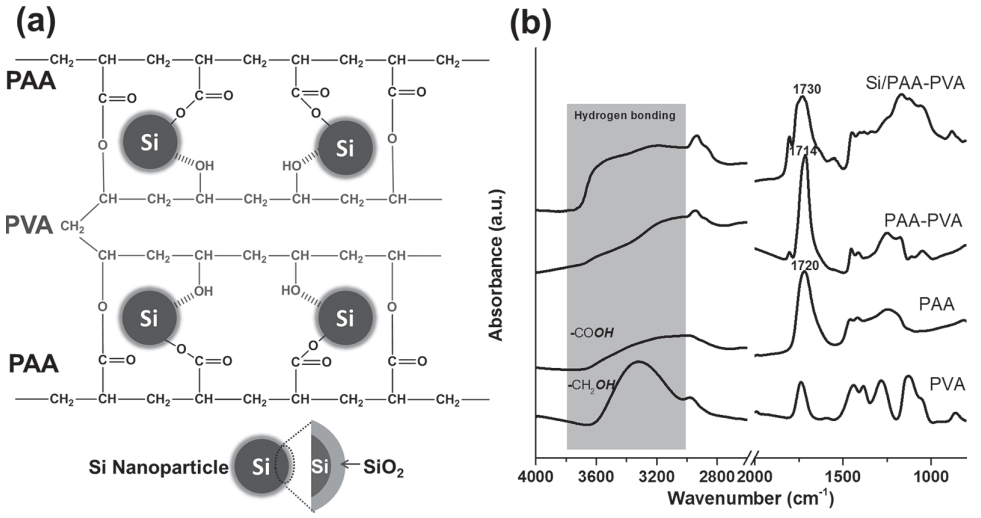

Figure 1. (a) The chemical structure and illustrative interaction between crosslined PAA-PVA and silicon particles; (b) FTIR spectra of PAA, PVA, PAA-PVA gel binder, and silicon/PAA-PVA composites.

and PVDF binder were prepared as control electrodes by following the same approach as the PAA-PVA binder.

As seen in the voltage profiles of the silicon electrode made with PAA-PVA binder (**Figure 2**a), the first cycle lithiation potential showed a plateau profile at 0.1–0.01 V, consistent with the behavior of crystalline Si.[28,49] The cycling stability and Coulombic efficiency of both the electrode and control electrodes, cycled at a current density of 400 mA/g, are shown in Figure 2b and c, respectively. For non-functional PVDF binder, the cell shows fast capacity fading (180 mAh/g after 50 cycles) with a very low initial Coulombic efficiency of 70.8%. The Si anode with functional NaCMC binder showed an initial capacity of 3282 mAh/g and a better cycling stability (1178 mAh/g after 100 cycles) compared to PVDF binder. Noticeably, the Si anode with the PAA-PVA binder exhibited an excellent battery performance. A specific capacity of 3616 mAh/g was achieved in the initial cycle by using novel interpenetrated gel polymer binder, which is about 86% of the theoretical capacity (4200 mAh/g). Furthermore, this cell also gave an excellent cycling stability, with a capacity of 2283 mAh/g remaining after 100 cycles. Moreover, this novel binder also showed a relatively high initial Coulombic efficiency of 83.9%, which increased to ~97.7% at the third cycle, and finally stabilized at ~99.3% in subsequent cycles. The high Coulombic efficiency of the silicon anode made with this interpenetrated gel polymer binder indicated a relatively stable SEI layer on the silicon particles, which prevents the loss of some irreversible lithium storage sites. This will also make the PAA-PVA gel binder more promising for the application of full-cell configuration that requires high Coulombic efficiency of both anodes and cathodes to advance the overall energy density and cycle life.

The fast charge/discharge further validates the reliability of the binders during a rapid substantial expansion and contraction for silicon nanoparticles.[50,51] Thus, we further evaluated the silicon electrode with the PAA-PVA binder at a rather high current density of 4 Ah/g as shown in **Figure 3**a. A high capacity of ~2660 mAh/g was obtained at this high current density of 1C (1C = 4000 mA/g). More importantly, the cell exhibited excellent cyclability with a high capacity of 1830 mAh/g remaining after 300 cycles, which corresponds to 68.6% capacity retention and only 0.1% capacity loss per cycle. The excellent battery

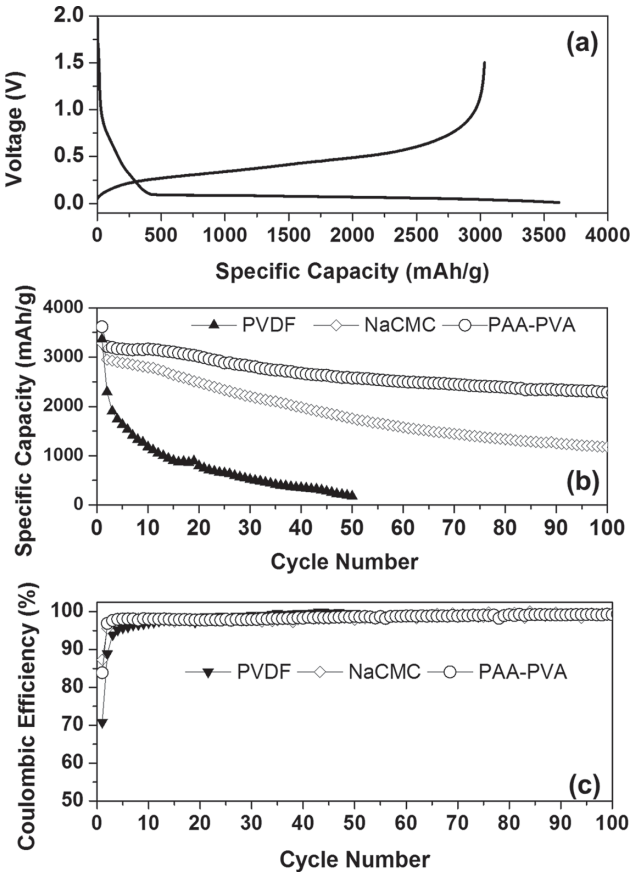

Figure 2. (a) The initial charge/discharge voltage profiles of the silicon anode using PAA-PVA gel polymer binder; (b) the cycling performance and (c) Coulombic efficiency of Si electrodes with PAA-PVA, NaCMC, and PAA binders. Note that the specific capacity is calculated based on silicon.

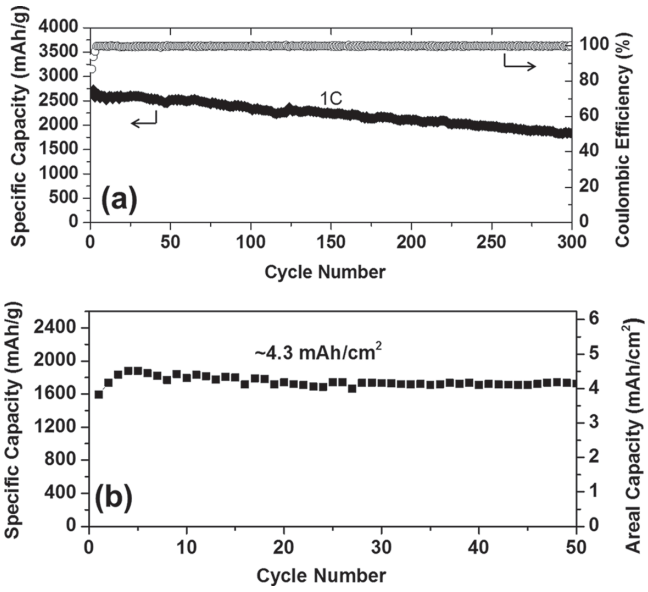

Figure 3. (a) The cycling stability and Coulombic efficiency of the silicon anode with PAA/PVA binder at a current density of 4 A/g (1C); (b) The cycle stability of silicon anodes with a high mass loading of 2.4 mg-Si/cm^2.

performance characteristics of the silicon electrode with PAA-PVA gel binder, such as high capacity retention and high Coulombic efficiency with long extended cycling at high current density, are outstanding compared to other silicon anodes using commercial Si nanoparticles reported in the literature.[21,22,25,26,52–54]

In practical applications, not only the specific capacity but also the mass loading of active material is crucial for achieving high energy density in batteries. Increasing mass loading of active materials on current collector can minimize the weight portion of the inactive parts (current collector, separator, and binder), and thus enhances the overall energy density of batteries. Areal capacity of electrodes, calculated as specific capacity (mAh/g) of active materials × mass loading (g/cm^2 of electrode area), is widely used for evaluation of electrode performance for practical application. It is clear that achieving a high areal capacity requires high mass loading in the electrodes.[7,13] Commonly, the specific capacity is highly dependent on the silicon loading, and will drop with increasing silicon loading because of higher polarization of the electrodes and poor adhesion of polymer binder.[32] Most of the high specific capacities reported in the literature for Si electrodes fabricated using coating techniques were obtained at a low silicon loading (below 1.5 mg-Si/cm^2).[21,22,25,26,52–54] This loading is insufficient to achieve an energy density greater than that of current graphite anodes in commercial LIBs. For this work, the electrode with a high mass loading of 2.4 mg/cm^2 still presents great cycling ability and the reversible capacity remains at around 1800 mAh/g up to 50 cycles. The silicon anode can deliver an areal capacity of ~4.3 mAh/cm^2, which is much higher than that of most reported silicon anode.[21,22,25,26,52–54]

To better understand the much-improved electrochemical performance achieved by using the interpenetrated gel polymer binder, scanning electron microscopy (SEM) was performed on the silicon electrodes with different binders before and after cycling. **Figure 4**a–c show the morphology of pristine electrodes with PVDF, NaCMC, and PAA-PVA binders, respectively. It was found that silicon nanoparticles together with carbon black were relatively uniformly dispersed in the matrix in the three samples at their origin state. Obvious morphology changes were observed for these electrodes after 100 cycles, shown in Figure 4d and 4e. The cycled electrodes using PVDF and NaCMC binders show smooth surface topography on some areas of the electrode surface, as marked by arrows in Figure 4d and 4e. The smooth surface is considered to be due to pulverization of silicon particles from substantial volume change and consequent growth of SEI on newly exposed surfaces.[32,55] In comparison, neither obviously detectable morphology change

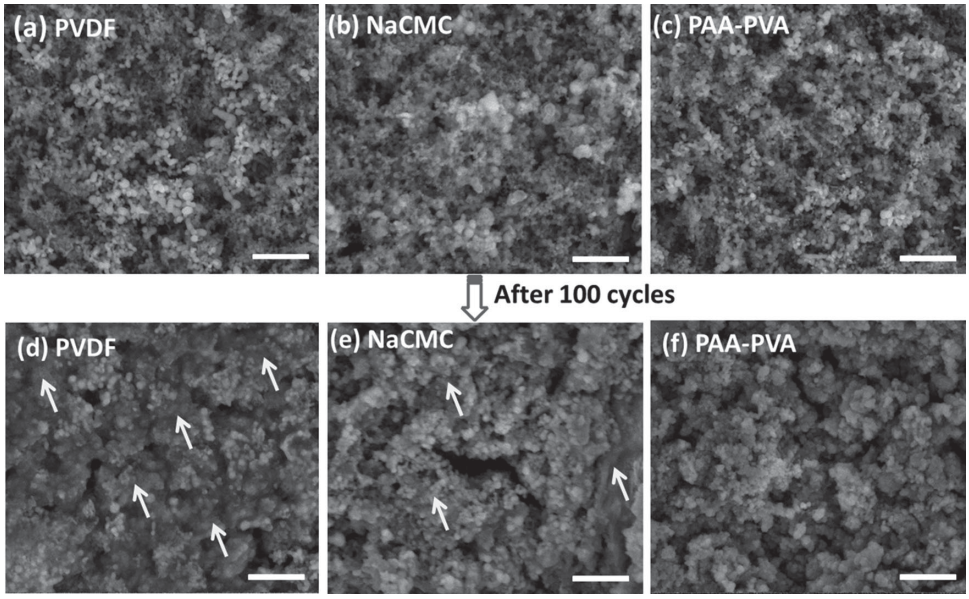

Figure 4. The surface morphology of silicon electrodes before and after 100th cycle using different binders. Scale bars in the images are 1 μm.

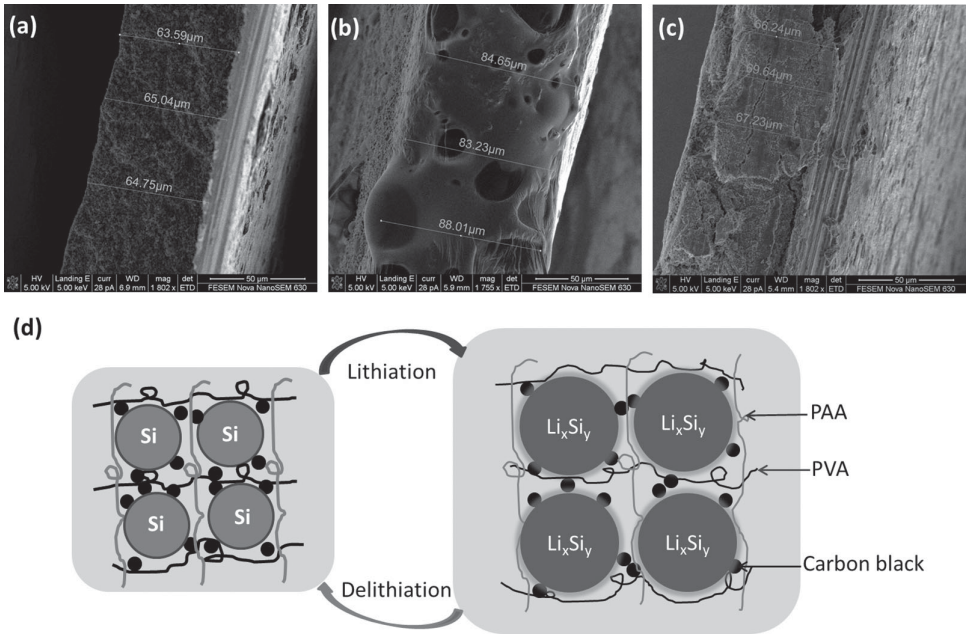

Figure 5. Cross-sectional SEM images of the silicon electrodes with gel-polymer binder (a) before cycling; (b) at the end of the 5th discharge and (c) at the end of the 5th charge; (d) proposed working mechanism of interpenetrated gel binder for silicon anodes.

nor microstructural failure was found for the electrode with the PAA-PVA binder, even after 100 deep cycles. Thus, the SEI layers on the silicon particles with PAA-PVA binder is believed to be thinner and more stable than those formed when using PVDF and NaCMC binder. The formation of the thin and stable SEI could be attributed to the novel polymer binder which accommodates the large volume change because of the deformable feature of the polymer network; furthermore, the enhanced adhesion stemming from strong chemical bonding between PAA-PVA and silicon nanoparticles should assist in constructing a stable SEI for Si electrodes. This bonding is similar to the hydrogen bonds of reported functionalized polymer binders for Si anodes.[33,39] The stable SEI is anticipated to play an active role in the cycle life and Coulombic efficiency, which directly lead to the excellent capacity retention with Coulombic efficiency over 99% of the Si anode with the PAA-PVA binder, as mentioned before (Figure 2).

The thickness variation of the silicon electrode using PAA-PVA binder with high silicon loading (~2.4 mg/cm^2) was further measured to validate the ability of the binder for accommodating large volume changes during cycling. **Figure 5**a–c show cross-section SEM images of electrodes before cycling, at the end of the 5th discharge, and at the end of the 5th charge, respectively. The thickness of discharged electrode (Figure 5b) increased to ca. 85.3 μm from its origin state (ca. 64.5μm) after lithiation, which is a ~32% volume change. Upon charging, the expanded silicon nanoparticles shrink as lithium is extracted; the final thickness of the electrode (67.4 μm) almost returns to its origin thickness with a volume variation of ~4.5%. By contrast, Figure S3 shows that the thickness of the silicon electrodes after cycling with PVDF and NaCMC binder increased by ~19.7% and ~16.5%, respectively, which are ~4 times higher than the increase with PAA-PVA gel polymer binder. The minimal thickness change of the electrodes with gel polymer binder after the cycle is due to the three-dimensional interpenetrated network of PAA-PVA binder which allows the reversible deformable change upon the volume change of Si during cycling.

To further evaluate the effect of PAA-PVA binder on Si composite anodes, the electrochemical properties of a silicon-graphite (Si-G) composite were also studied. The composite composed of silicon and graphite with a mass ratio of 6:4 was used as the active material. The electrode was fabricated using an industrially used coating technique with the active material (Si-G composites), carbon black, and binder ratio of 90:5:5 (weight ratio). Here, only 5% binder was used to achieve maximum energy density for practical applications. **Figure 6** shows the cycling stability of Si-G composite electrodes at a current

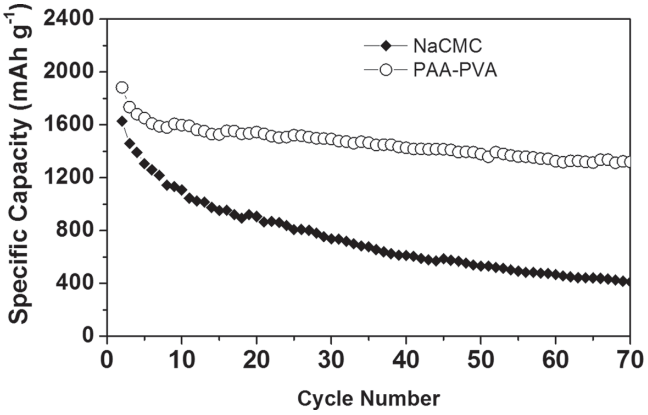

Figure 6. The cycling stability of silicon-graphite (Si-G) composite anode (Si:Graphite = 6:4, mass ratio) using NaCMC and PAA-PVA gel polymer binder. The electrode was composed of Si-G composites (90%), super P (5%), and polymer binder (5%). Note that the specific capacity is calculated based on silicon.

density of 400 mA/g. The PAA-PVA binder shows a high utilization of active composites (Si-G) with a reversible capacity of 1880 mAh/g at the first cycle and a good capacity retention of 70% after 70 cycles. In contrast, the cells using NaCMC binder only show a capacity retention of 25%, much lower than PAA-PVA. This result further demonstrated that the water soluble, interpenetrated gel polymer binder has a good compatibility with commercial Si-graphite mixture-based anodes, which makes it more promising for practical application.

3. Conclusion

We have developed an interpenetrated gel polymer binder for high performance silicon anodes by using a facile in-situ thermal-crosslinking technique based on the low-cost water soluble poly(acrylic acid) (PAA) and polyvinyl alcohol (PVA) precursors. By having the advantages of a deformable polymer network and strong binding between Si and the binder, this designed binder can effectively accommodate the large volume change of silicon anode upon lithiation/delithiation, resulting in an excellent cycling stability (1663 mAh/g after 300 cycles) and high Coulombic efficiency (99.3%) even at a high current density of 4 A/g. Furthermore, high-areal-capacity of 4.3 mAh/cm^2 with good cycling stability was demonstrated at electrode level using the silicon anode based on the PAA-PVA binder. This much improved electrochemical performance is attributed to the interpenetrated gel network of this binder and its strong chemical bonding with silicon particles. In addition, it also can assist in the formation of stable SEI layers of silicon anode. Taking the facile solution fabrication process and the eco-friendly and low-cost qualities into account, this novel developed water soluble interpenetrated gel binder has a great potential to be used for high capacity silicon anodes in next generation lithium-ion batteries, and also may be extended to other electrode materials that undergo large volume change.

4. Experimental Section

Materials Characterization: FTIR spectroscopy was performed as diffuse reflectance measurements with powder samples using a Bruker IFS 66/S FT-IR spectrometer and Spectra-Tech Collector II DRIFTS accessory. The surface morphologies and thickness of the silicon electrodes before and after cycling were investigated with a NanoSEM 630 scanning electron microscope .

Electrode Fabrication and Electrochemical Measurement: The aqueous solution of mixed Poly(arylic acid) (Alfa Aesar, Average Mw = 240 000) and Poly(vinyl alcohol) (Aldrich, Average Mw = 31 000) with the weight ratio of 9:1 was developed as gel polymer binder for silicon anodes. For comparison purpose, the polyvinylidene fluoride (PVDF) solution of *N*-methyl-2-pyrrolidone (NMP) and aqueous sodium carboxymethyl cellulose (NaCMC) were used control binders. Typically, nano-sized Si powder (Alfa Aesar, <100 nm), conducting additives, and polymer binder with the weight ratio of 6:2:2 were ball-milled for 2 h to form uniform slurry, followed by coating slurries on copper foil using a doctor blade. Afterwards, the silicon electrode was thermal treatment at 100 °C for 5 h and then increased to 150 °C for another 1 h under vacuum. Super P carbon black was used as conducting agent for low-mass-loading electrode, while Super P carbon black/carbon nanofiber mixture (1:1, weight ratio) was used for high-mass-loading electrodes. Electrochemical tests were performed by using 2016 coin-type half cells assembled with lithium metal as the counter electrode in Argon filled glove box. The electrolyte consisted of 1 mol/L LiPF6 in a mixture of ethylene carbonate, diethyl carbonate and dimethyl carbonate (EC: DEC: DMC, 1:1:1 by volume) and fluoroethylene carbonate (FEC, 10 vol%). The FEC additive can increase the cycling efficiency of silicon anodes, due to the formation of a more stable SEI layer. Galvanostatic cycling test was carried out at different constant current densities between 0.01 and 1.5 V vs Li/Li+ on a BT2000 battery testing system (Arbin Instruments, USA). The specific capacity was calculated on the basis of the weight of the active materials.

Supporting Information

Supporting Information is available from the Wiley Online Library or from the author.

Acknowledgements

J. Song and M. Zhou contributed equally to this work. This work was supported by the Assistant Secretary for Energy Efficiency and Renewable Energy, Office of Vehicle Technologies of the U.S. Department of Energy under Contract No. DE-EE0006447.

Received: April 20, 2014
Revised: June 2, 2014
Published online: July 19, 2014

[1] J. M. Tarascon, M. Armand, *Nature* **2001**, *414*, 359–367.
[2] J. B. Goodenough, Y. Kim, *Chem. Mater.* **2009**, *22*, 587–603.
[3] M. S. Whittingham, *Chem. Rev.* **2004**, *104*, 4271–4301.
[4] M. Armand, J. M. Tarascon, *Nature* **2008**, *451*, 652–657.
[5] A. S. Arico, P. Bruce, B. Scrosati, J. M. Tarascon, W. Van Schalkwijk, *Nat. Mater.* **2005**, *4*, 366–377.
[6] B. Dunn, H. Kamath, J.-M. Tarascon, *Science* **2011**, *334*, 928–935.
[7] T. Xu, J. Song, M. L. Gordin, H. Sohn, Z. Yu, S. Chen, D. Wang, *ACS Appl. Mater. Inter.* **2013**, *5*, 11355–11362.
[8] J. Liu, J.-G. Zhang, Z. Yang, J. P. Lemmon, C. Imhoff, G. L. Graff, L. Li, J. Hu, C. Wang, J. Xiao, G. Xia, V. V. Viswanathan, S. Baskaran, V. Sprenkle, X. Li, Y. Shao, B. Schwenzer, *Adv. Funct. Mater.* **2013**, *23*, 929–946.
[9] Y. Shao, F. Ding, J. Xiao, J. Zhang, W. Xu, S. Park, J.-G. Zhang, Y. Wang, J. Liu, *Adv. Funct. Mater.* **2013**, *23*, 987–1004.
[10] J. Qian, X. Wu, Y. Cao, X. Ai, H. Yang, *Angew. Chem. Int. Ed.* **2013**, *52*, 4633–4636.
[11] W. J. Li, S. L. Chou, J. Z. Wang, H. K. Liu, S. X. Dou, *Nano Lett.* **2013**, *13*, 5480–5484.
[12] J. Song, Z. Yu, T. Xu, S. Chen, H. Sohn, M. Regula, D. Wang, *J. Mater. Chem. A* **2014**, *2*, 8623–8627.
[13] J. Song, T. Xu, M. L. Gordin, P. Zhu, D. Lv, Y.-B. Jiang, Y. Chen, Y. Duan, D. Wang, *Adv. Funct. Mater.* **2014**, *24*, 1243–1250.
[14] C.-M. Park, J.-H. Kim, H. Kim, H.-J. Sohn, *Chem. Soc. Rev.* **2010**, *39*, 3115–3141.
[15] W.-J. Zhang, *J. Power Sources* **2011**, *196*, 13–24.
[16] Y. Kim, Y. Park, A. Choi, N. S. Choi, J. Kim, J. Lee, J. H. Ryu, S. M. Oh, K. T. Lee, *Adv. Mater.* **2013**, *25*, 3045–3049.
[17] A. Darwiche, C. Marino, M. T. Sougrati, B. Fraisse, L. Stievano, L. Monconduit, *J. Am. Chem. Soc.* **2012**, *134*, 20805–20811.
[18] M. R. Zamfir, H. T. Nguyen, E. Moyen, Y. H. Lee, D. Pribat, *J. Mater. Chem. A* **2013**, *1*, 9566–9586.
[19] U. Kasavajjula, C. Wang, A. J. Appleby, *J. Power Sources* **2007**, *163*, 1003–1039.

[20] H. Wu, Y. Cui, *Nano Today* **2012**, *7*, 414–429.
[21] C. Chae, H.-J. Noh, J. K. Lee, B. Scrosati, Y.-K. Sun, *Adv. Funct. Mater.* **2014**, *24*, 3036–3042.
[22] X. Chen, K. Gerasopoulos, J. Guo, A. Brown, C. Wang, R. Ghodssi, J. N. Culver, *Adv. Funct. Mater.* **2011**, *21*, 380–387.
[23] J.-Y. Choi, D. J. Lee, Y. M. Lee, Y.-G. Lee, K. M. Kim, J.-K. Park, K. Y. Cho, *Adv. Funct. Mater.* **2013**, *23*, 2108–2114.
[24] X. H. Liu, L. Zhong, S. Huang, S. X. Mao, T. Zhu, J. Y. Huang, *ACS Nano* **2012**, *6*, 1522–1531.
[25] J. R. Szczech, S. Jin, *Energy. Environ. Sci.* **2011**, *4*, 56–72.
[26] N. Liu, H. Wu, M. T. McDowell, Y. Yao, C. Wang, Y. Cui, *Nano Lett.* **2012**, *12*, 3315–3321.
[27] H. Wu, G. Chan, J. W. Choi, I. Ryu, Y. Yao, M. T. McDowell, S. W. Lee, A. Jackson, Y. Yang, L. Hu, Y. Cui, *Nature Nano* **2012**, *7*, 310–315.
[28] J. Song, S. Chen, M. Zhou, T. Xu, D. Lv, M. L. Gordin, T. Long, M. Melnyk, D. Wang, *J. Mater. Chem. A* **2014**, *2*, 1257–1262.
[29] R. Yi, F. Dai, M. L. Gordin, S. Chen, D. Wang, *Adv. Energy Mater.* **2013**, *3*, 295–300.
[30] M. Zhou, M. L. Gordin, S. Chen, T. Xu, J. Song, D. Lv, D. Wang, *Electrochem. Commun.* **2013**, *28*, 79–82.
[31] S. Chen, M. L. Gordin, R. Yi, G. Howlett, H. Sohn, D. Wang, *Phys. Chem. Chem. Phys.* **2012**, *14*, 12741–12745.
[32] N. Liu, Z. Lu, J. Zhao, M. T. McDowell, H.-W. Lee, W. Zhao, Y. Cui, *Nature Nano* **2014**, *9*, 187–192.
[33] I. Kovalenko, B. Zdyrko, A. Magasinski, B. Hertzberg, Z. Milicev, R. Burtovyy, I. Luzinov, G. Yushin, *Science* **2011**, *334*, 75–79.
[34] H. Wu, G. Yu, L. Pan, N. Liu, M. T. McDowell, Z. Bao, Y. Cui, *Nat. Commun.* **2013**, *4*, 1943.
[35] C. Wang, H. Wu, Z. Chen, M. T. McDowell, Y. Cui, Z. Bao, *Nat. Chem.* **2013**, *5*, 1042–1048.
[36] C. Marino, L. Boulet, P. Gaveau, B. Fraisse, L. Monconduit, *J. Mater. Chem.* **2012**, *22*, 22713.
[37] C. Marino, A. Debenedetti, B. Fraisse, F. Favier, L. Monconduit, *Electrochem. Commun.* **2011**, *13*, 346–349.
[38] S. Komaba, N. Yabuuchi, T. Ozeki, Z.-J. Han, K. Shimomura, H. Yui, Y. Katayama, T. Miura, *J. Phys. Chem. C* **2012**, *116*, 1380–1389.
[39] A. Magasinski, B. Zdyrko, I. Kovalenko, B. Hertzberg, R. Burtovyy, C. F. Huebner, T. F. Fuller, I. Luzinov, G. Yushin, *ACS Appl. Mater. Inter.* **2010**, *2*, 3004–3010.
[40] D. Munao, J. W. M. van Erven, M. Valvo, E. Garcia-Tamayo, E. M. Kelder, *J. Power Sources* **2011**, *196*, 6695–6702.
[41] S. Komaba, K. Shimomura, N. Yabuuchi, T. Ozeki, H. Yui, K. Konno, *J. Phys. Chem. C* **2011**, *115*, 13487–13495.
[42] M.-H. Ryou, J. Kim, I. Lee, S. Kim, Y. K. Jeong, S. Hong, J. H. Ryu, T.-S. Kim, J.-K. Park, H. Lee, J. W. Choi, *Adv. Mater.* **2013**, *25*, 1571–1576.
[43] M. Wu, X. Xiao, N. Vukmirovic, S. Xun, P. K. Das, X. Song, P. Olalde-Velasco, D. Wang, A. Z. Weber, L.-W. Wang, V. S. Battaglia, W. Yang, G. Liu, *J. Am. Chem. Soc.* **2013**, *135*, 12048–12056.
[44] B. Koo, H. Kim, Y. Cho, K. T. Lee, N.-S. Choi, J. Cho, *Angew. Chem. Int. Ed.* **2012**, *51*, 8762–8767.
[45] S. Scognamillo, V. Alzari, D. Nuvoli, A. Mariani, *J. Polym. Sci. Part A* **2010**, *48*, 2486–2490.
[46] Y. Zhao, H. J. Su, L. Fang, T. W. Tan, *Polymer* **2005**, *46*, 5368–5376.
[47] S. M. M. Quintero, R. V. Ponce, F. M. Cremona, A. L. C. Triques, A. R. d'Almeida, A. M. B. Braga, *Polymer* **2010**, *51*, 953–958.
[48] Y. Lu, D. Wang, T. Li, X. Zhao, Y. Cao, H. Yang, Y. Y. Duan, *Biomaterials* **2009**, *30*, 4143–4151.
[49] H. Wu, G. Zheng, N. Liu, T. J. Carney, Y. Yang, Y. Cui, *Nano Lett.* **2012**, *12*, 904–909.
[50] H. Kim, B. Han, J. Choo, J. Cho, *Angew. Chem.Int. Ed.* **2008**, *120*, 10305–10308.
[51] X. Chen, X. Li, F. Ding, W. Xu, J. Xiao, Y. Cao, P. Meduri, J. Liu, G. L. Graff, J.-G. Zhang, *Nano Lett.* **2012**, *12*, 4124–4130.
[52] H. Wu, G. Zheng, N. Liu, T. J. Carney, Y. Yang, Y. Cui, *Nano Lett.* **2012**, *12*, 904–909.
[53] H. C. Tao, L. Z. Fan, X. Qu, *Electrochim. Acta* **2012**, *71*, 194–200.
[54] Y.-S. Hu, R. Demir-Cakan, M.-M. Titirici, J.-O. Müller, R. Schlögl, M. Antonietti, J. Maier, *Angew. Chem. Int. Ed.* **2008**, *47*, 1645–1649.
[55] C. K. Chan, H. Peng, G. Liu, K. McIlwrath, X. F. Zhang, R. A. Huggins, Y. Cui, *Nature Nano* **2008**, *3*, 31–35.